Copyright © 2005 American Scientific Publishers
All rights reserved
Printed in the United States of America

Journal of
Nanoscience and Nanotechnology
Vol. 5, 1683–1687, 2005

RESEARCH ARTICLE

Optical and Field Emission Properties of Zinc Oxide Nanostructures

Hui Pan,[1] Yanwu Zhu,[1] Zhenhua Ni,[1] Han Sun,[1] Cheekok Poh,[1] Sanhua Lim,[1] Chornghaur Sow,[1] Zexiang Shen,[1] Yuanping Feng,[1] and Jianyi Lin[1,2,*]

[1] *Department of Physics, National University of Singapore, 2 Science Drive 3, Singapore 117542*
[2] *Institute of Chemical and Engineering Sciences, 1 Pesek Road, Jurong Island, Singapore 627833*

Zinc Oxide (ZnO) nano-pikes were produced by oxidative evaporation and condensation of Zn powders. The crystalline structure and optical properties of the ZnO nanostructures (ZnONs) greatly depend on the deposition position of the ZnONs. TEM and XRD indicated that the ZnONs close to the reactor center, ZnON-A, has better crystalline structure than the ZnONs away from the center, ZnON-B. ZnON-A showed the PL and Raman spectra characteristic of perfect ZnO crystals, whereas ZnON-B produced very strong green emission band at 500 nm in the photoluminescence (PL) spectrum and very strong Raman scattering peak at 560 cm^{-1}, both related to the oxygen deficiency due to insufficient oxidation of zinc vapor. ZnON-B exhibited better field emission properties with higher emission current density and lower turn-on field than ZnON-A.

Keywords: ZnO Nanostructures, Photoluminescence, Field Emission Properties.

1. INTRODUCTION

ZnO possesses spectacular chemical, structural, electrical and optical properties that make it useful for a diverse range of technological applications. As a wide band gap semiconductor (3.37 eV at room temperature) with large exciton binding energy (60 meV), ZnO is of great interest for the applications in low-voltage and short-wavelength electric and photonic devices, such as blue and UV light emitting diodes for full-color display and room-temperature excitonic ultraviolet laser diodes for high density optical storage.[1–4] Like many semiconductor materials, nanostructured ZnO may have superior optical properties than bulk crystals because of the quantum confinement effects.[1,4–8] Therefore the study of nanostructured ZnO has received increasing attention. A variety of ZnO nanostructural (ZnON) morphologies have been reported, including nanowires,[1] nanobelts,[9] nanocombs,[10] nanosprings,[11] nanorings,[12] nanotubes,[13] and nanocrystals.[14] Many methods have been employed in the synthesis of nanostructural ZnO, such as template (anodic aluminum oxide) growth,[15] catalytic vapor phase transport process,[16,17] solution deposition,[4,14,18,19] thermal evaporation and condensation of Zn-containing materials (ZnO,[20] zinc halide,[21] or metallic Zn powder in the presence of oxygen),[22] metal organic vapor deposition,[23,24] laser molecular beam epitaxy,[25] plasma-enhanced molecular beam epitaxy[2] and ion sputter deposition,[26] etc. When the thermal evaporation and condensation process was used, the structure and morphology of ZnO were found to depend on the location of deposition.[20] In this paper, ZnO nanostructures were produced by the oxidization of Zn powder via thermal evaporation. The nanostructured ZnO formed under insufficient oxidation conditions were shown to have strong photoluminescence in green light region and better field emission with lower turn-on field.

2. EXPERIMENTAL DETAILS

Nanostructured ZnO was prepared by thermal vaporization and condensation of Zn (99.9% purity) power in the presence of oxygen. The alumina boat with Zn powder was placed at the center of a quartz tube reactor (80 cm in length, 2.5 cm in diameter). The tube was purged by a Helium (99.999% purity) flow with 100 standard cubic centimeters per minute (sccm). The furnace temperature

*Author to whom correspondence should be addressed.

 1533-4880/2005/5/1683/005 doi:10.1166/jnn.2005.183

was increased to 850 °C, and an oxygen (99.99% purity) flow was introduced to the tube reactor at a flow rate of 10 sccm. The mixed O_2 and He gas was maintained throughout the whole reaction process, which usually takes 30 minutes. After the reaction, the O_2 flow was switched off. The reactor was cooled down to room temperature with the protective He flow.

The morphologies of as-grown ZnO nanostructures (ZnONs) were observed on a scanning electron microscope (SEM, JEOL JSM-6700F) and high resolution transmission electron microscope (HRTEM, JEOL 2010). The crystalline structures of ZnONs were further characterized by XRD (Brucker AXS D8). Photoluminescence in the visible region was recorded on a computer-controlled spectrofluorometer (Jasco FP-6300) at room temperature. A high intensity Xenon lamp at 160 W power is used as the light source. Raman scattering of the as-grown ZnONs was measured by using micro-Raman Renishaw 2000 system (with 1 cm^{-1} resolution and 0.4 cm^{-1} reproducibility, at the excitation source of 514.5 nm).

The measurements of field emission (FE) properties of ZnONs were carried out using two-parallel-plate set-up in a high vacuum of about 5×10^{-7} Torr.[27] The peeled ZnON films were adhered onto the Cu substrate, which serves as cathode, by double-sided copper tape. Indium tin oxide (ITO) glass covered with a layer of phosphor was employed as the anode. A polymer plate was used as a spacer and the distance between the electrodes was kept at 100 μm. A Keithley 237 high voltage source measurement unit (SMU) was used to apply a voltage from 0 to 1100 V and to measure the emission current at the same time. All the measurements were performed at room temperature.

(a)

(b)

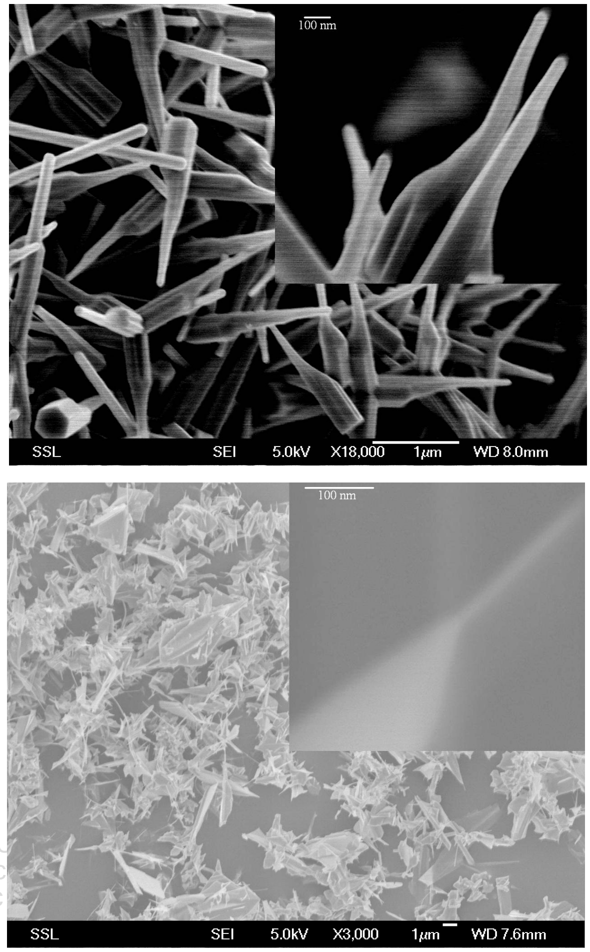

Fig. 1. SEM images of ZnON: (a) ZnON-A and (b) ZnON-B. The insets in the figures show close-up view of the pike tip at higher magnifications.

3. RESULTS AND DISCUSSION

The ZnONs were obtained at the two different locations. ZnON-A was deposited on the reactor wall in the zone close to the center of the reaction tube (around 750 °C) while ZnO-B was produced in the zone close to the gas outlet (around 200 °C). Figure 1a shows a SEM image of ZnON-A. The pike-shaped structure is observable, with a hexagonal bottom of about 200 nm in diameter and a sharp tip of less than 50 nm in diameter (see the inset in Fig. 1a). The average length of the ZnON-A pikes is about 1.5 μm. The X-ray diffraction pattern in Figure 2a is characteristic of the wurtzite-structure ZnO. The selected-area electron diffraction (SAED) taking from one isolated ZnO nanofibre under TEM (see Fig. 3) indicates that the ZnON-A is basically single crystalline with some poly-crystalline mixture. Figure 1b shows the SEM image of ZnON-B, in which the nano-pikes become thinner with the tip less than 10 nm in diameter (see the inset in Fig. 1b) and mixed with leaf-shaped ZnO. The XRD pattern of ZnON-B in Figure 2b shows that the ZnON-B sample possesses wurtzite structure. However several weak peaks in Figure 2b indicate the existence of Zn particles in ZnON-B. This is understandable since ZnON-B was collected from the reactor wall away from the center of the furnace, where the temperature was relatively low. The zinc vapor may not be fully oxidized and the nano ZnO pikes formed are thinner. At the place close to the center of the reactor, the temperature is high with sufficient Zn vapor and O_2, so that larger nano ZnO pikes of higher crystalline quality were produced.

The photoluminescence (PL) of ZnONs at room temperature is shown in Figures 4a and 4b with the excitation wavelength of 325 nm. For ZnON-A, one dominant peak at 383 nm (corresponding to 3.26 eV) is observable (Fig. 4a). This UV emission band can be attributed to the ZnO near-band exciton emission. This peak is similar to the P peak previously reported on high-quality ZnO crystals at warm temperature.[8, 28–30] When the ZnO crystal is warmed, the shallow bound excitons de-trap thermally, and the inelastic scattering of free excitons would result in the observation of the P peak.[30] For ZnON-B, in addition to the above two PL peaks, a very strong and broad band is centered at 500 nm. This green emission

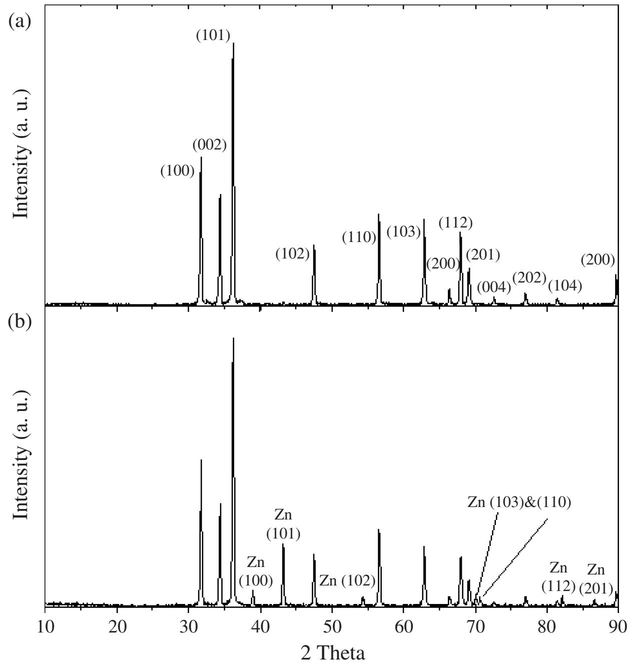

Fig. 2. XRD patterns for: (a) ZnON-A and (b) ZnON-B.

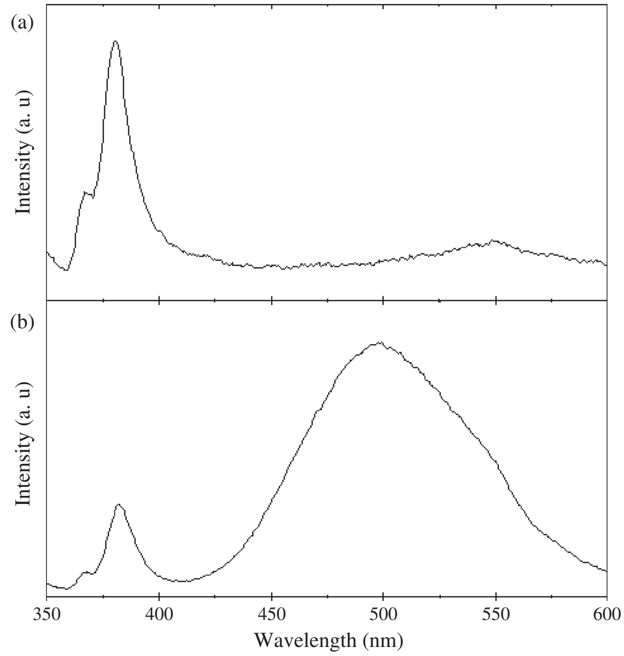

Fig. 4. Photoluminescence spectra obtained using Xenon lamp at 160 W as excitation source for: (a) ZnON-A and (b) ZnON-B.

(around 2.46 eV) was proposed to be due to defects-form deep centers (oxygen vacancies as discussed in following Raman scattering)[8, 19, 23, 31, 32] which trap electrons (or holes). These defects may largely occur in the imperfect grain boundary sites as well as other interstitial defects in ZnO. ZnON-B which was formed from the incomplete oxidation of zinc vapor is expected to consist of large amount of defects and hence shows very strong green PL emission. ZnON-A shows no green PL emission.

Raman scattering spectra are shown in Figures 5a and 5b. According to Group theory[33–35] zinc oxide with hexagonal wurtzite structure belongs to C_{6v}^4 ($P6_3$ mc) space group and may have the following normal lattice vibration modes: $\Gamma_{opt} = A_1 + 2B_1 + E_1 + 2E_2$. Among them A_1, E_1 and E_2 are Raman active whereas B_1 is forbidden. From selection rules, only A_1 and E_2 modes can be observed in unpolarized Raman spectra. Hence the peaks at 332 cm^{-1}, 381 cm^{-1}, and 437 cm^{-1} in Figure 5a for ZnON-A can be assigned to E_2 (low), A_1, and E_2 (high), respectively.[35]

Delivered by Publishing Technology to: University of Waterloo
IP: 216.240.78.203 On: Tue, 13 Oct 2015 21:08:07
Copyright: American Scientific Publishers

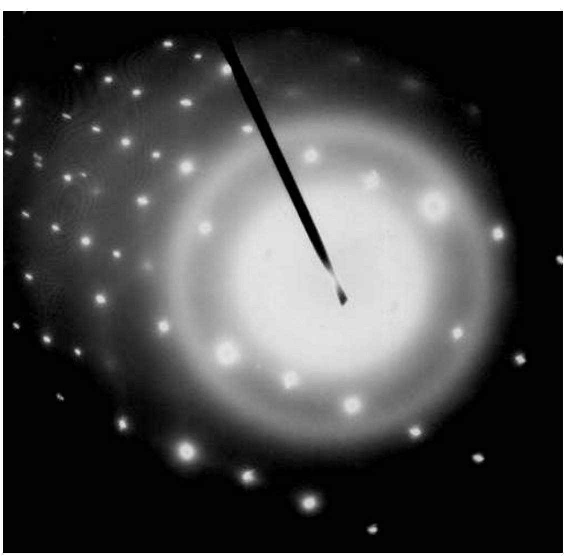

Fig. 3. Selective area electron diffraction pattern of ZnON-A.

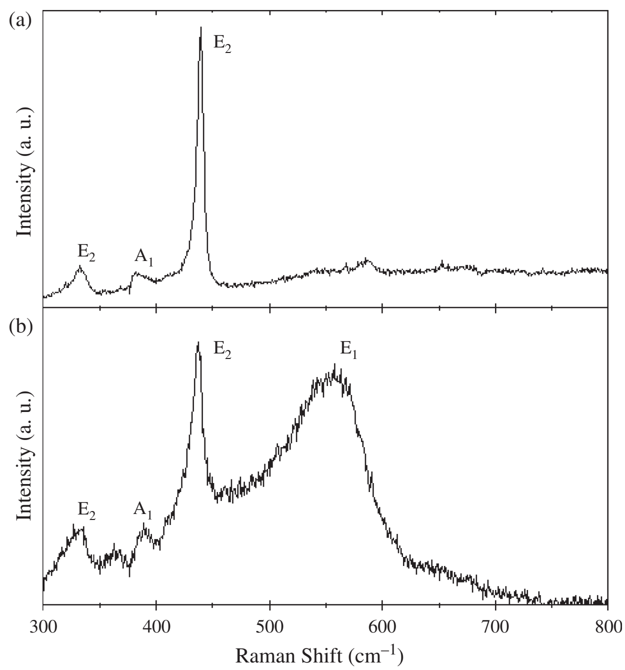

Fig. 5. Raman spectra with the excitation of 514.5 nm laser light for: (a) ZnON-A and (b) ZnON-B.

RESEARCH ARTICLE

RESEARCH ARTICLE

In Figure 5b ZnON-B produces a broad strong band at 560 cm^{-1}. This Raman band is known to be related to the E_1 mode due to the oxygen deficiency.[36,37] The Raman spectra of the samples further confirmed the oxygen vacancies in ZnON-B.

The field emission current density as a function of the macroscopic electric field is shown in Figure 6. The turn-on fields for the two samples are 5.0 V/μm (ZnON-A) and 4.5 V/μm (ZnON-B), respectively. The emission current density reached 0.07 mA/cm^2 for ZnON-B at 7 V/μm, which is much higher than that of ZnON-A (0.02 mA/cm^2 at 11 V/μm). The Fowler–Nordheim (FN) plots for the measured samples are shown in the inset in Figure 6. It is clear that the measured data fit well with the FN equation:[38]

$$\ln\left(\frac{J}{E^2}\right) = \ln\left(\frac{A\beta^2}{\varphi}\right) - \frac{B\varphi^{3/2}}{\beta E} \quad (1)$$

where J is the emission current density (A cm^{-2}), E is the applied field (V μm^{-1}), $A = 1.543 \times 10^{-6}$ A eV V^{-2}, $B = 6.833 \times 10^3$ $eV^{-3/2}$ Vμm^{-1}, β is the field enhancement factor, and φ is the work function of emitter material (5.3 eV for ZnO).[39] The calculated field enhancement factor β from the slope of the inset in Figure 6 is 1320 for ZnON-A and 1370 for ZnON-B, respectively. The β value of nanostructural ZnO is related to the geometry, crystal structure, conductivity, work function, and nanostructure density. The field emission current density of the ZnON-B is better than or at least comparable with those reported in literature for well-aligned ZnO nanofibers ($\beta = 847$),[38] although our samples were randomly oriented.[39] It should be mentioned that our field emission results are worse than those of ZnO nanowires on carbon fibers[40] with enhanced conductivity and alignment. The nanopikes in ZnON-B exhibit very sharp tip (Fig. 1b). The oxygen deficiency as indicated from the PL (Fig. 4b) and Raman spectra (Fig. 5b) may enhance the conductivity of the ZnON-B (the measured resistance of ZnON-B is much smaller than that of ZnO-A). And the density of ZnON-B is lower than that of ZnON-A. All these factors contribute to the high emission current density and high field enhancement factor of ZnON-B.

Delivered by Publishing Technology to: University of Waterloo
IP: 216.240.76.203 On: Tue, 13 Oct 2015 21:08:07
Copyright: American Scientific Publishers

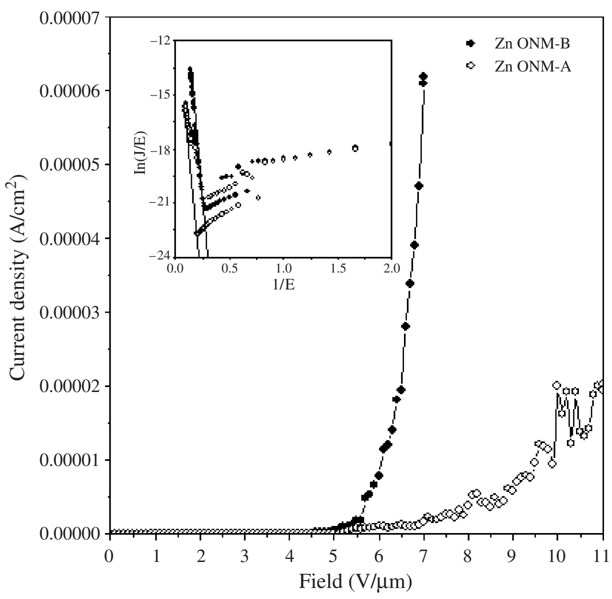

Fig. 6. Field emission results for ZnON-A (open symbols) and ZnON-B (solid symbols).

4. CONCLUSIONS

In summary, ZnO nano-pike structures were produced by oxidative evaporation and condensation of Zn powders. The purity and crystalline structures of the ZnONs samples were related to the deposition positions. High quality crystalline ZnONs were produced at the place close to the center of the reactor. They have the PL and Raman spectra characteristic of perfect ZnO crystals. The ZnON-B produced at the place close to the gas outlet has oxygen vacancies as indicated by the additional peaks in PL and Raman spectra due to insufficient oxidation of Zn vapor. ZnON-B gives a strong green PL emission and exhibits excellent field emission properties with high emission current density and lower turn-on field.

References and Notes

1. M. H. Huang, S. Mao, H. Feick, H. Yan, Y. Wu, H. Kind, E. Weber, R. Russo, and P. Yang, *Science* 292, 1897 (**2001**).
2. D. M. Bagnall, Y. F. Chen, Z. Zhu, T. Yao, S. Koyama, M. Y. Shen, and T. Goto, *Appl. Phys. Lett.* 70, 2230 (**1997**).
3. H. Cao, J. Y. Xu, D. Z. Zhang, S. H. Chang, S. T. Ho, E. W. Seelig, X. Liu, and R. P. H. Chang, *Phys. Rev. Lett.* 84, 5584 (**2000**).
4. M. H. Huang, Y. Wu, H. Feick, N. Tran, E. Weber, and P. Yang, *Adv. Mater.* 13, 113 (**2001**).
5. E. M. Wong and P. C. Searson, *Appl. Phys. Lett.* 74, 2939 (**1999**).
6. B. J. Jin, S. H. Bae, S. Y. Lee, and S. Im, *Mater. Sci. Eng. B* 71, 301 (**2000**).
7. C. Pieralli and M. Hoummady, *Appl. Phys. A* 66, 377 (**1998**).
8. Y. Gu, I. L. Kuskovsky, M. Yin, S. O'Brien, and G. F. Neumark, *Appl. Phys. Letts.* 85, 3833 (**2004**).
9. Z. W. Pan, Z. R. Dai, and Z. L. Wang, *Science* 291, 1947 (**2001**).
10. S. Hashimoto and A. Yamaguchi, *J. Am. Ceram. Soc.* 79, 1121 (**1996**).
11. X. Y. Kong and Z. L. Wang, *Nano Lett.* 3, 1625 (**2003**).
12. X. Y. Kong, Y. Ding, R. S. Yang, and Z. L. Wang, *Science* 303, 1348 (**2004**).
13. J. Zhang, L. Sun, C. Liao, and C. Yan, *Chem. Commun.* 262 (**2002**).
14. R. Viswanatha, S. Sapra, B. Satpati, P. V. Satyam, B. N. Dev, and D. D. Sarma, *J. Mater. Chem.* 14, 661 (**2004**).
15. Y. Li, G. M. Meng, L. D. Zhang, and F. Phillipp, *Appl. Phys. Lett.* 76, 2011 (**2000**).
16. Y. W. Wang, L. D. Zhang, G. Z. Wang, X. S. Peng, Z. Q. Chu, and C. H. Liang, *J. Cryst. Growth* 234, 171 (**2002**).
17. C. N. R. Rao, G. Gundiah, F. L. Deepak, A. Govindaraj, and A. K. Cheetham, *J. Mater. Chem.* 14, 440 (**2004**).
18. D. S. Boyle, K. Govender, and P. O'Brien, *Chem. Commun.* 80 (**2002**).
19. M. Yin, Y. Gu, I. L. Kuskovsky, T. Andelman, Y. Zhu, G. F. Neumark, and S. OBrien, *J. Am. Chem. Soc.* 126, 6206 (**2004**).

20. J. Lee, K. Park, M. Kang, I. Park, S. Kim, W. K. Cho, H. S. Han, and S. Kim, *J. Crystal Growth* 254, 423 **(2003)**.
21. K. Omichi, N. Takahashi, T. Nakamura, M. Yoshioka, S. Okamoto, and H. Yamamoto, *J. Mater. Chem.* 11, 3158 **(2001)**.
22. H. Yan, R. He, J. Johnson, M. Law, R. J. Saykally, and P. Yang, *J. Am. Chem. Soc.* 125, 4728 **(2003)**.
23. B. P. Zhang, N. T. Binh, Y. Segawa, Y. Kashiwaba, and K. Haga, *Appl. Phys. Lett.* 84, 586 **(2004)**.
24. B. Zhao, H. Yang, G. Du, X. Fang, D. Liu, C. Gao, X. Liu, and B. Xie, *Semicond. Sci. Technol.* 19, 770 **(2004)**.
25. C. H. Chia, T. Makino, K. Tamura, Y. Segawa, M. Kawasaki, A. Ohtomo, and H. Koinuma, *Appl. Phys. Lett.* 82, 1848 **(2003)**.
26. W. Chiou, W. Wu, and J. Ting, *Diamond and Related Materials* 12, 1841 **(2003)**.
27. Y. W. Zhu, T. Yu, F. C. Cheong, X. J. Xu, C. T. Lim, V. B. C. Tan, J. T. L. Thong, and C. H. Sow, *Nanotechnology* 16, 88 **(2005)**.
28. Y. C. Kong, D. P. Yu, B. Zhang, W. Fang, and S. Q. Feng, *Appl. Phys. Lett.* 78, 407 **(2001)**.
29. B. P. Zhang, K. Wakatsuki, N. T. Binh, Y. Segawa, and N. Usami, *J. Appl. Phys.* 96, 340 **(2004)**.
30. J. Wilkinson, G. Xiong, K. B. Ucer, and R. T. Williams, *J. Nonlinear Optics* 29, 529 **(2002)**.
31. K. Vanheusden, W. L. Warren, C. H. Seager, D. K. Tallant, J. A. Voigt, and B. E. Gnade, *J. Appl. Phys.* 79, 7983 **(1996)**.
32. D. Li, Y. H. Leung, A. B. Djurisic, Z. T. Liu, M. H. Xie, S. L. Shi, S. J. Xu, and W. K. Chan, *Appl. Phys. Lett.* 85, 1601 **(2004)**.
33. A. Kaschner, U. Haboeck, M. Strassburg, G. Kaczmarczyk, A. Hoffmann, C. Thomsen, A. Zeuner, H. R. Alves, D. M. Hofmann, and B. K. Meyer, *Appl. Phys. Lett.* 80, 1909 **(2002)**.
34. M. Tzolov, N. Tzenov, D. D. Malinovska, M. Kalitzova, C. Pizzuto, G. Vitali, G. Zollo, and I. Ivanov, *Thin Solid Films* 379, 28 **(2000)**.
35. F. Decremps, J. P. Porres, A. M. Saitta, J. C. Chervin, and A. Polian, *Phys. Rev. B* 65, 092101 **(2002)**.
36. X. L. Xu, S. P. Lau, J. S. Chen, G. Y. Che, and B. K. Tay, *J. Cryst. Growth* 223, 201 **(2001)**.
37. J. J. Wu and S. C. Liu, *J. Phys. Chem. B* 106, 9546 **(2002)**.
38. C. J. Lee, T. J. Lee, S. C. Lyu, Y. Zhang, H. Ruh, and H. J. Lee, *Appl. Phys. Lett.* 81, 3648 **(2002)**.
39. C. C. Tang and Y. Bando, *Appl. Phys. Lett.* 83, 659 **(2003)**.
40. D. Banerjee, S. H. Jo, and Z. F. Ren, *Adv. Mater.* 16, 2028 **(2004)**.

Received: 1 February 2005. Accepted: 15 April 2005.

RESEARCH ARTICLE

Delivered by Publishing Technology to: University of Waterloo
IP: 216.240.76.203 On: Tue, 13 Oct 2015 21:08:07
Copyright: American Scientific Publishers